

Research

Hot-Cell Examination of a Defect Rod from IFA-597

Tord Jonsson

November 1998

Research

Hot-Cell Examination of a Defect Rod from IFA-597

Tord Jonsson

Studsvik Nuclear AB
SE-611 82 Nyköping
Sweden

November 1998

This report concerns a study which has been conducted for the Swedish Nuclear Power Inspectorate (SKI). The conclusions and viewpoints presented in the report are those of the author/authors and do not necessarily coincide with those of the SKI.

SUMMARY

The examined test rod from Halden was refabricated at Kjeller from fuel rod 33-25065 previously irradiated in Ringhals 1 1980-1992. The heat rating was low during the later part of the irradiation in Ringhals 1. The refabricated test rod failed when the linear heat rate was increased from 23,7 to 28,3 kW/m.

The failed rod had a long axial crack. The total length of the crack was 377 mm, which is somewhat more than the length of the fuel column.

The cracks in the cladding have started in the outer part of the cladding and propagated inwards. The cracks have started at several different axial positions. This indicates that the power profile during the test was relatively flat.

SAMMANFATTNING

Den undersökta teststaven från Halden var refabricerad i Kjeller från bränslestav 33-25065, som bestrålades i Ringhals 1 1980-92. Bränslestavens effekt i Ringhals 1 var låg under den senare delen av bestrålningen. Den refabricerade staven gick sönder när den lineära belastningen ökade från 23,7 till 28,3 kW/m.

Den skadade staven hade en lång axiell spricka. Den totala längden av sprickan var 377 mm, vilket är något mer än bränslepelarens längd.

Sprickorna i kapslingen hade startat på kapslingens utsida och propagerat inåt. Sprickorna har startat vid flera axiella positioner, vilket tyder på att den axiella effektprofilen var relativt jämn.

1998-11-16

6385

Tord Jonsson

SKI No 14.6-960821:97102

Hot-Cell examination of a defect rod from IFA-597

Final report

SKI No 14.6-960821:97102

Summary

The examined test rod from Halden was refabricated at Kjeller from fuel rod 33-25065 previously irradiated in Ringhals 1 1980-1992. The heat rating was low during the later part of the irradiation in Ringhals 1. The refabricated test rod failed when the linear heat rate was increased from 23,7 to 28,3 kW/m.

The failed rod had a long axial crack. The total length of the crack was 377 mm, which is somewhat more than the length of the fuel column.

The cracks in the cladding have started in the outer part of the cladding and propagated inwards. The cracks have started at several different axial positions. This indicates that the power profile during the test was relatively flat.

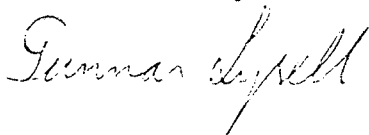
Sammanfattning

Den undersökta teststaven från Halden var refabricerad i Kjeller från bränslestav 33-25065, som bestrålades i Ringhals 1 1980-92. Bränslestavens effekt i Ringhals 1 var låg under den senare delen av bestrålningen. Den refabricerade staven gick sönder när den lineära belastningen ökade från 23,7 till 28,3 kW/m.

Den skadade staven hade en lång axiell spricka. Den totala längden av sprickan var 377 mm, vilket är något mer än bränslepelarens längd.

Sprickorna i kapslingen hade startat på kapslingens utsida och propagerat inåt. Sprickorna har startat vid flera axiella positioner, vilket tyder på att den axiella effektprofilen var relativt jämn.

Reviewed by



Approved by



1998-11-16

List of contents

	Page	
1	Introduction	1
2	Data from manufacturing and irradiation	2
3	Examinations	3
3.1	Neutron radiography	3
3.1.1	Method	3
3.1.2	Results	3
3.2	Gamma measurements	4
3.2.1	Method	4
3.2.2	Results	4
3.3	Profilometry	5
3.3.1	Method	5
3.3.2	Results	5
3.4	Visual inspection	6
3.4.1	Method	6
3.4.2	Results	6
3.5	Optical microscopy	9
3.5.1	Method	9
3.5.2	Results	9
3.6	Examination of polished cross section in SEM (including determination of hydrogen content)	11
3.6.1	Method	11
3.6.2	Results	12
3.7	Fractography (SEM)	13
3.7.1	Method	13
3.7.2	Results	13
4	Discussion	15
5	Acknowledgement	16
	References	16
Table		
1	Positions of specimens for destructive examinations	
Appendices		
A1	Neutron radiography	
B1-B2	Gamma measurements	
C1-C2	Profilometry	
D1-D6	Visual inspection	
E1-E13	Optical microscopy	
F1-F8	SEM examination of polished surfaces	
G1-G12	SEM examination of fracture surfaces	
H1	Positions of specimens for destructive examinations	

1998-11-16

1 Introduction

Two rods in IFA-597.2 were refabricated from fuel rod 33-25065 irradiated in Ringhals 1. The irradiation of the father rod in Ringhals was prolonged to "two lives" to reach high burnup.

The objective of the test at Halden was to study the thermal behaviour and the fission gas release of high burnup commercial BWR-LWR fuel. The rods in the test were instrumented with fuel centreline thermocouples and bellows pressure transducers.

Fuel rod 5 in IFA-597.2 failed during the test at Halden. The rod is marked 597-9 from the manufacturing. The failed rod was transported to Studsvik for post irradiation examination. The main purpose of the examination was a study of the failure. The examination of the failed rod, described in this report, was financed by SKI (the Swedish Nuclear Power Inspectorate).

1998-11-16

2 Data from manufacturing and irradiation

The examined test rod was refabricated at Kjeller from a power reactor rod. The father rod 33-25065 was manufactured by ABB Atom AB and irradiated in Ringhals 1 during an extended time from 1980 to 1992 to an average burnup of 58,5 MWd/kgU. The linear heat rate during the last year of the irradiation in Ringhals was less than 5 kW/m. The rod was examined at Studsvik after the irradiation in Ringhals 1 and three parts of the rod were transported to Kjeller in Norway. The rodlet was manufactured from segment D5:3 in the father rod. This segment was cut from a region fairly high up in the father rod (between the 4th and 5th spacers). The refabricated rodlet was marked IFA-597-9, and was equipped with a centreline thermocouple and pressure transducer.

The rod IFA-597-9 was irradiated as rod 5 in Halden assembly IFA-597.2. The irradiation test in the Halden reactor was performed in July 1995. Four ramps were performed with the assembly IFA-597.2. The maximum linear heat rate in rod 5 during the first three ramps were 19,5, 18,7 and 16,5 kW/m respectively. The linear heat rate in the fourth ramp was increased in three steps. The rod was intact after an increase of the linear heat rate to 23,1 kW/m and failed in connection with an increase to 28,3 kW/m. A third increase was performed to a linear heat rate of 30,6 kW/m and the irradiation was continued with the rod in a defect condition during 8 days [1].

The test in Halden was performed in the reactor coolant (D₂O), which has a pressure of 30 bar. The boiling temperature of the coolant is about 240 °C.

1998-11-16

3 Examinations

The following examinations were performed in Studsvik on rod 5 from IFA-597.2.

1. Neutron radiography
2. Gamma measurements
3. Profilometry
4. Visual inspection
5. Optical microscopy of fuel and cladding, 2 cross-sections
6. SEM examination of cladding, including measurement of hydrogen-deuterium content, 1 cross section
7. SEM examination of fracture surfaces, 2 specimens

The positions for destructive examinations are shown in Appendix H1.

3.1 Neutron radiography

3.1.1 Method

The rod was mounted in a watertight aluminium capsule in the hot cells. The capsule was transported to the R2-reactor. The capsule was placed in the radiography equipment, which was then emptied of water to give the neutrons free passage from the reactor. The surfaces of the radiography chamber were allowed to dry for some hours to avoid disturbing water droplets. A dysprosium foil, which was placed behind the capsule, was then exposed for about 30 minutes. During exposure Dy-164 was transformed to the β -active isotope Dy-165 (half-life about 2 hours). The dysprosium foil was placed in contact with a photographic film, which was exposed by the β -irradiation. The photographic film was developed in the normal way.

3.1.2 Results

Reproductions from the radiography are shown in Appendix A1. The axial positions of the plenum and the fuel column from the neutron radiography are presented in section 3.4.2 and Table 1.

No local concentrations of hydrogen in the cladding can be observed. There is an $\approx 16,5$ mm long part of the cladding near the lower end of the rod where the oxide was removed in connection with the refabrication. The cladding temperature will be lower in such a region and hydrogen diffusion to such an area is likely to occur in spite of the low coolant temperature in the

1998-11-16

Halden reactor. The neutron radiography does not reveal an increased hydrogen content even in this region or at the ends of the fuel column.

There are some regions along the crack in the cladding with increased attenuation of the thermal neutrons (less blackening of the radiographic film). This phenomenon is interpreted as the presence of a reaction product between the UO_2 fuel and water on the surface of the exposed fuel. The reaction product, schoepite contains hydrogen and gives a large contrast in neutron radiography.

3.2 Gamma measurements

3.2.1 Method

The measurements were performed using a Ge-detector and a 0,5 mm collimator. The gamma spectra are measured and analysed at equidistant positions along the rod.

3.2.2 Results

Plots from the gamma measurements are shown in Appendices B1-B2.

No comments on the power distribution during the irradiation in Halden can be given, based on the gamma measurements, due to the long time between the irradiation and the measurement.

The axial distributions of Cs-134 and Cs-137 are very irregular due to loss of Cs during the irradiation with a long crack in the cladding (Appendix B1).

The axial distribution of Eu-154 shows that the loss of fuel is very small (Appendix B2). Eu-154 has low mobility in the fuel and a high energy gamma peak (1274 keV) was used in the measurement. The lower Eu-154 activity in the top end of fuel is due to the removal of UO_2 in the central parts of the pellets for insertion of the thermocouple.

The Co-60 activity originates mainly from crud deposited on the cladding during the irradiation in Ringhals 1. A region in the lower part, where the crud and oxide layer was removed in connection with refabrication is very conspicuous by the lack of Co-60 (Appendix B2). The highest Co-60 activity occurs in the lower part of the rod immediately below the UO_2 fuel and is caused by a spring in the gas plenum.

1998-11-16

3.3 Profilometry

3.3.1 Method

A vertical profilometer rig was used. The diameter measurement system was calibrated prior to the measurements against two standards with different diameters.

Spiral scans were performed.

The output signal can be plotted both directly and after passing a low-pass filter. The filtered curve shows the average diameter. Both diameter and ovality can be observed on the unfiltered curves.

The uncertainty of the diameter traces is according to our experience, less than $\pm 5 \mu\text{m}$.

3.3.2 Results

A plot from the profilometry without low pass filter and a pitch of 4 mm/turn is shown in Appendix C1. A curve with this large pitch gives the possibility to observe the variation of the diameter during the rotation. The ovality (difference between maximum and minimum) is plotted in Appendix C2.

The curve in Appendix C1 shows that the angular extensions of the minima are small and that the angular extensions of the maxima are larger. In connection with the measurement it was observed that the minima correspond to the angle with diameters through the crack in the rod.

The diameter decrease due to creep-down of the cladding was larger than the diameter increase due to oxidation during the base irradiation in Ringhals 1. The diameter of the rod was thus about 0,035 mm less than the nominal as fabricated diameter, when post-irradiation examination was performed in Studsvik in 1993.

Appendices C1 and C2 show that the diameter increase from the original manufactured diameter 12,25 mm is large along the fuelled part of the rod. The diameter increase over most of the fuelled sections average 0,35-0,55 mm.

There is a small region on the rod near the lower end where the diameter seems to be uninfluenced by the refabrication and the test in the Halden reactor. This region is positioned in the plenum part between the branched lower end of the crack and above the region where the oxide was removed in connection with the refabrication (Photo in Appendix D1). The diameter here is 12,21-12,22 mm along a length of about 4 mm.

1998-11-16

The largest diameter occurs in the upper part of the rod. The axial position of the largest diameters corresponds to the second and third pellet below the central thermocouple. The average diameter and the ovality are also larger in the same region (Appendices C1 and C2).

The largest measured diameters are about 12,85 mm corresponding to a diameter increase of 0,6 mm from the nominal manufactured diameter. The maximum ovality amounts to about 0,3 mm.

A local minimum in the lower part of the rod (about 159-175 mm from the lower end of the rod in Appendix C2) is evidently caused by the removal of crud and outer oxide layer in this area in connection with the refabrication of the rodlet.

3.4 Visual inspection

3.4.1 Method

A Hensholdt periscope in conjunction with a visual fixture was used for the inspection. The fuel rod is fastened on the visual fixture, which is driven by stepping motors under the periscope. The motion can be both translational and rotational. The rod can also be rotated at the same time as it is moved horizontally so that the rod is observed during a spiral movement. Pictures were taken with a digital camera through the periscope.

The axial position can be determined with an accuracy of $\pm 0,1$ mm and the angular accuracy is $\pm 10^\circ$.

3.4.2 Results

Photos from the examination are shown in Appendices D1-D6.

The rod has an axial crack along the main part of the cladding. The axial extent of the crack is 377 mm, which can be compared with the length of the fuel column, 361 mm according to the neutron radiography. The neutron radiography also showed that the rod has a 19 mm long plenum at the lower end of the rod and that there is an about 1 mm large gap between the upper end of the fuel column and the upper end plug.

1998-11-16

Comparison of axial positions from visual inspection and neutron radiography (distances from lower end of the rod):

<u>Neutron Radiography</u>	<u>Visual inspection</u>
Plenum 128-147 mm	Branched crack 135,4-147,4 mm
Fuel 147-508 mm	Unbranched crack 147,4-512,4 mm

The comparison shows that the extension of the axial crack is larger than the UO₂ fuel column both at the upper and lower ends. The crack extends upwards into the region of the top end plug. The branching into two cracks in the lower end of the rod occurs close to the border between the UO₂ fuel column and the plenum.

The opening of the crack is about 1,5 mm along the main part of the crack length. The size of the opening corresponds to a diameter increase of about $1,5/\pi$ mm or about 0,5 mm. This is close to the average measured diameter increase. The diameter increase is mainly due to the opening of the crack and significantly less than 0,05 mm of the diameter increase is caused by plastic deformation of the cladding, corresponding to less than 0,4 % strain.

Numerous light patches on the cladding surface are due to local spalling of oxide from the cladding surface. No such spalling was observed after the base irradiation in Ringhals and the spalling has evidently occurred during the test in the Halden reactor. The spalling was presumably caused by deformation of the cladding during the Halden test.

Metallography in Studsvik of specimens from the sibling rod from Ringhals 1 showed nodular corrosion of the cladding. The corrosion is nodular also in this rod. This is clearly visible in regions of the cladding where the outer oxide layer was removed in connection with the refabrication. Only the even oxide layer was removed and light patches due to remaining oxide can be observed at the locations with thicker oxide (Appendices D1, D4 and D5).

The wide opening of the axial crack makes it possible to inspect the fracture surface by visual examination. The direction for the axial propagation of the crack is however difficult to observe except at a few positions.

The crack orientation is mainly axial. There is one major irregularity, ~286 mm from the lower end (Appendix D2). The neutron radiography does not show any increased hydrogen content in the cladding there and the axial crack has apparently not started at this position. It seems more likely that this step is a position where two axial cracks have met.

1998-11-16

The crack surface is perpendicular to the outer surface in the outer part of the cladding but has an inclined angle in the inner part. The area with the perpendicular crack surface is in some regions small (Appendix D6, photo 3).

The fracture sometimes has an appearance, which is reminiscent of axial propagation due to delayed hydride cracking. These positions where the axial direction of propagation can be observed are:

- near the upper end of the axial crack (Appendix D4, photo 3) and
- in a branch at the large step in the middle of the rod (Appendix D6, photo 1)
- at both sides of the branching at the lower end of the axial crack (one of these positions is shown in Appendix D5, photo 1)

The striations show the direction of propagation and not consecutive positions of the propagation front. At the top end of the fuel column the fracture has evidently propagated upwards and the striations show that the propagation front extends further up at the outer side of the cladding. Similar conclusions can be made for the fracture at the position for the step in the axial crack ~286 mm from the lower end, whereas the direction of propagation is more complex in the region for branching in the lower end of the rod.

The visible striations indicate that the direction of crack propagation is nearly perpendicular to the cladding surface along the main part of the rod and the propagation is from the outer side towards the inner side. The starting point(s)/region(s) of the axial crack was not identified by the visual inspection of the fracture surfaces. A likely explanation for the difficulty to identify the positions for the start of the axial crack is that the crack started at several axial positions. The axial crack is however localised near one generatrix of the rod and this requires an explanation. The crack is in some regions remarkably straight (e.g. Appendix D1 photo 2 and Appendix D2 photo 3). This appears to be due to the fact that the cracks have started at positions with scratches in the cladding from the original mounting of the fuel rod in the fuel assembly. These scratches are visible in photos 1 and 2 in Appendix D2.

Minor cracks beside the main crack were observed about 166 mm (Appendix D5, photo 3) and 417 mm from the lower end (Appendix D3, photo 3). It was suspected early during the examination that the axial cracks had started at these observed locations with minor cracks beside the main crack, which could explain two axial cracks meeting each other about 286 mm from the lower end of the rod.

The outer oxide layer appears to have some influence on the crack propagation. The fracture is different, with numerous steps, at the position where the

1998-11-16

outer oxide layer was removed in connection with the refabrication at Kjeller (Appendix D1). The difference is however only partial. Steps occur also at other axial positions but are less conspicuous in regions with thick outer oxide. The minor cracks beside the main crack shown in Appendix D5, photo 3 are located at positions of oxide nodules in the outer oxide layer.

The positions for the start of the axial cracks in the cladding are also discussed in chapters 3.7.2 and 4.

Some unidentified shiny material can be observed through the crack near the upper end of the rod - material from the thermocouple?

3.5 Optical microscopy

Two cross sections including cladding and fuel were examined. The positions were chosen at the two axial positions with visible cracks beside the main crack. The axial positions are shown in Appendix H1.

3.5.1 Method

50 mm long sections were taken at the chosen axial positions. The sections were impregnated and mounted in epoxy resin. The impregnated specimens were cut close to the desired observation plane with cracks beside the main crack. The specimens were ground and polished. The final polishing step was performed using colloidal silica which provides a flat and deformation free surface.

The oxide on the cladding and the porosity of the fuel was examined after the final polishing step. The cladding was then etched and examined for hydrides and finally the fuel was etched to study the grain structure.

The microscopy was performed using a Reichert Telatom-3 optical microscope.

3.5.2 Results

Appendices E1- E7 show photos from the examination of a cross section 417 mm from the lower end of the rod (specimen 1804). Photos from the visual inspection at the same axial position are shown in Appendices D3.

Appendix E1 shows the total cross section with a wide opening in the cladding. The loss of UO_2 fuel appears to be small in agreement with the gamma

1998-11-16

measurements. The sum of the widths of the cracks in the outer part of the fuel is about equal to the width of the crack in the cladding.

The width and number of radial cracks in the fuel decreases sharply about 1,2 mm inwards from the cladding. It is evident that swelling of a central plastic part of the fuel has been the driving force for enlarging the width of the crack and that the central hole in the fuel was formed by gas bubbles moving towards the centre due to the thermal gradient.

The visual inspection showed spalling of the outer oxide layer (Appendices D1-D4). The metallography shows an oxide layer with numerous small cracks. A fairly thin outer part of the oxide layer is absent due to spalling in some areas (Appendix E2).

Appendix E3 shows hydrides in the cladding after etching. The cladding contains many radial hydrides especially in the outer part of the cladding. These hydrides were redistributed during the Halden irradiation and can be supposed to be perpendicular to stresses in the cladding. At the cracks, both penetrating and non-penetrating, there are numerous hydrides perpendicular to the crack surface. These hydrides orthogonal to the crack surfaces show orientation of stresses after the formation of the cracks and not during the crack propagation.

Appendix E4 shows photos from the rim zone in the outer part of the fuel and a partly damaged bonding zone between fuel and cladding.

Appendix E5 shows the structure along a radius in the fuel from centre to periphery and Appendices E6 and E7 show photos with higher magnification before and after etching along the same radius.

Appendices E8- E13 show photos from the examination of a cross section 166 mm from the lower end of the rod (specimen 1805). Photos from the visual inspection at the same axial position are shown in Appendices D1 (photo D.1.1) and D5 (photo D.5.3).

Appendix E8 shows the total cross section with a wide opening in the cladding. Examination of the specimen after additional grinding and polishing, not shown in the Appendices, showed that the apparent loss of UO₂ fuel is due to cracks in the pellet parallel with the specimen surface.

The central zone with increased porosity is smaller in this specimen (Appendix E8) than in the previous specimen (Appendix E1). The radial cracks in the outer part of the fuel also extend further inwards in this specimen (about 2 mm). The explanation is either lower temperature (caused by lower linear heat rating) or less oxidation of the fuel in this part of the rod.

1998-11-16

There is no oxide layer on the outer surface apart from a few nodules in agreement with photos in Appendices D1 and D6.

Appendix E9 shows hydrides in the cladding after etching (the appearance of the cladding is somewhat changed due to regrinding and repolishing of the specimen). The same comment can be given about the hydrides in this specimen as for specimen 1804.

Appendix E10 shows photos from the rim zone in the outer part of the fuel and a partly damaged bonding zone between fuel and cladding.

Appendix E11 shows the structure along a radius in the fuel from centre to periphery and Appendix E12 and E13 show photos before and after etching along the same radius with higher magnification.

3.6 Examination of polished cross section in SEM (including determination of hydrogen content)

A specimen 383 mm from the lower end of the rod was examined. This means that the specimen is fairly close to specimen 1804 for optical microscopy and immediately above specimen 1802 for examination of the fracture surface in SEM (See Appendix H1).

3.6.1 Method

A sample of the cladding was embedded in epoxy resin. The final polishing step was performed using colloidal silica, which provides a flat and deformation-free surface. The specimen was coated with gold and transferred to the scanning electron microscope. The gold coating prevents charging near the edges of the specimen. The thickness of the gold layer is estimated to 4 nm according to the manufacturer of the Emitech K250 sputter coater.

The specimen was examined in a JEOL JXA-840 scanning electron microscope with a tetragonal backscatter detector (LINK) of high sensitivity. There is a (small) difference in average atomic number between the hydrides, the oxides and the metallic matrix. It is necessary to use a relatively high electron beam current to ensure good contrast. Using a short working distance and low accelerating voltage would increase resolution, but also increase the electron channelling contrast, which in this case would make the image analysis troublesome. A relatively high accelerating voltage (20 kV) and long working distance (15 mm) produces an image without electron channelling contrast, which can be analysed for hydride or oxide with good results.

1998-11-16

The hydride and oxide images were collected on a VIDAS image analysing system (Zeiss Kontron) and analysed at a later stage. Hydride images were collected from the outside to the inside of the cladding at 1000x. Seven images covered the entire wall thickness, without overlap. In order to reliably evaluate the area fraction of the hydrides, the grey scale of the image was stretched out to fill up the available range {0 (black) to 255 (white)}. The grey scale image was then segmented into a binary image consisting of objects (hydrides) and not-objects (matrix). The area fraction (F) of the hydrides was then measured in each image.

The major part of the hydrogen in the cladding exists as relatively large precipitated hydrides in normally cooled power reactor fuel rods. For the interpretation of the measurements it was further assumed that the hydrides are the δ -phase with 62 atomic % H and have a density of 5,65 g/cm³. 62 atomic % H corresponds to 17 570 ppm H. If the hydrogen occurs as light hydrogen and not as deuterium, the hydrogen content (c_H , weight-ppm of hydrogen) can be calculated by use of the following expression

$$c_H = 17570 \cdot 5,65F / (6,54 - 0,89F)$$

An average hydride concentration across the cladding thickness was calculated by weighting the hydride concentration at each radius with the area (volume) it occupies.

3.6.2 Results

Photos are shown in Appendices F1-F7. The penetrating crack is perpendicular to the outer surface a short distance in the outer part of the cladding and the final shear fracture comprises the main part of the clad thickness.

The orientation of the hydrides is mainly tangential but there are also some radial hydrides throughout the thickness of the cladding.

The measured hydrogen contents are shown in Appendix F8. The curves refer to different angular positions with the crack at 0°. Two of the curves refer to measurements close to the crack, one measurement on each side.

The average measured hydrogen content amounts to 290 ppm H equivalents. The measurements show somewhat higher hydrogen content in the vicinity of the crack. The angular variation in hydride concentration may be insignificant or caused by the temperature gradients after the formation of the crack and not necessarily an explanation for the localisation of the crack.

1998-11-16

The oxide thickness in the specimen is influenced by spalling of the oxide layer. Photo 1 and 2 in Appendix F3 show an oxide thickness of about 40 μm in a region without evident oxide spalling or local increase due to oxide nodules. This is in good agreement with data from the base irradiation and the specimen 1804 examined by optical microscopy (Appendix E2).

3.7 Fractography (SEM)

Two specimens of fracture surfaces were examined. One specimen was taken near the upper end of the long crack in the cladding. The other specimen was chosen 360-380 mm from the lower end of the rod.

3.7.1 Method

The specimens were examined in a JEOL JXA-840 scanning electron microscope. The specimens were cleaned in nitric acid after cutting and before preparation for the examination.

3.7.2 Results

Photos of specimen 1802, 360-380 mm from the lower end of the rod are shown in Appendices G1-G6. This specimen is immediately below the SEM cross section 1803 shown in Appendices F1-F7 and the cross section for optical microscopy 1804 shown in Appendices E1-E7.

Photos of specimen 1801, 487-507 mm from the lower end of the rod are shown in Appendices G7-G12. This specimen is near the upper end of the fuel part of the rod and within the region with annular pellets (for the central thermocouple).

The direction of the striations in specimen 1802 indicates that this specimen contains a starting region for the axial crack. The specimen contains practically the complete length of an axial crack and other cracks on the same generatrix have met near the ends of the specimen. The start of the crack and the axial propagation at the outer surface of the cladding can be supposed to be along a scratch on the surface from the mounting of the original assembly for the irradiation at Ringhals as discussed in section 3.4.2. The crack is very straight at the position of this specimen as observed in the visual inspection (left part of photo D.3.1 in Appendix D3).

The fracture surface is for both specimens nearly perpendicular to the cladding surface in the outer part and has an angle of about 45° to the cladding

1998-11-16

surface in the inner part. The fracture surface in the outer part has an appearance typical for delayed hydride cracking [3]. Striations in the surface indicate the direction of the propagation in this region. The direction of the striations is nearly perpendicular to the cladding surface along the main part of the two specimens. The axial direction of the propagation is easily observed in the upper part of the specimen 1801 (photos in Appendix G8).

The propagation is here upwards in the rod. The crack propagates faster near the outer surface and the front in axial direction is mostly very close to the outer surface and impossible to observe in the photos. The front for the axial propagation is deeper into the cladding at the position for the detail photos in Appendix G11. Different directions of the striations are easily observed in photo G8.2. A fish-bone pattern can be observed with propagation both to the left and towards the inner and outer surfaces of the cladding.

The axial positions of pellet-pellet interfaces were identified (photos in Appendices G6 and G12). The axial positions of the pellet-pellet interfaces are also indicated in Appendices G1, G3 and G7-G9.

The final shear crack is a small part of the crack surface in specimen 1802 (Appendix G1) and a large fraction of the crack surface in specimen 1801 (Appendix G7).

The photos in Appendices G5 and G11 show double bright contours at several locations. This is due to oxidation of the fracture surface. Edges can appear bright in SEM and the double bright lines here are due to double edges formed by oxidation of the surface. The oxide formed will not be even when a surface with an acute angle is oxidised. The new oxidised surface will instead contain two edges and the oxide thickness can be estimated from the distance between the two edges. The distance between the two lines in these photos is somewhat below 1 μm corresponding to oxide thickness on the surface of about the same size, which is in good agreement with photos of oxide on the fracture surface in Appendix F4.

The photos in Appendix G8 contain some artefacts. The horizontal lines in the left part of photo G8.1 is due to electrical charging of the specimen and there are some chips from the cutting of the specimen on the fracture surface in photo G8.2. One chip is shown in larger magnification in Appendix G12.

Cracks in the oxide layer on the inner side of the cladding are shown in photos G12.1 and G12.3 in Appendix G12. These cracks in the oxide layer were formed due to deformation of the cladding material in connection with the final propagation of the crack through the cladding.

1998-11-16

4 Discussion

The power excursion in this test is probably outside possible transients for a fuel rod with such a high burnup during normal power operation in a light water power reactor. The IFA rod failed at a comparatively low heat rating. This can be explained by a very small diametrical gap between fuel and cladding due to the high burnup and the very low heat rating during the later part of the irradiation in Ringhals 1. The low coolant temperature and fast neutron flux in the Halden reactor presumably prevented any significant cladding creep during the first power ramps.

The crack started at the outside of the cladding at several positions along the rod, initiated by scratches formed already at the time of mounting the original rod in the Ringhals 1 assembly.

A sister rod with the same data from the same assembly was ramped in the Studsvik R2 reactor in 1994 to 33 kW/m. The ramp rate in that case was 0,113 W/m/s or about twelve times slower than the ramp which caused the IFA 597-9 to fail. In the Studsvik ramps only incipient cracks to about one tenth of the cladding thickness were seen to have started from the inside. They were of the SCC type. Apart from the higher ramp rate for IFA 597-9 the cladding temperature difference between the two tests may have caused the different behaviour. The outside cladding temperature in the Studsvik test was 290 °C versus 244 °C for IFA 597-9.

The higher amount of precipitated hydrogen in the Halden test, due to the lower temperature, may be one of the factors explaining the different behaviour.

It was not possible to determine the axial power distribution from activity measurements at the time of the examination. General considerations on expected power distribution in a short fuel rod in a reactor makes it however likely that the highest power densities (W/gU) occurred at the ends of the rod. From the appearance of the axial crack it is likely that there are several starting points for the formation of the long axial crack. The localisation to one side of the rod is partly random (or due to an unidentified cause) and partly due to localisation to scratches in the cladding surface from the mounting of the rod into the original fuel assembly irradiated in Ringhals.

The first defect in the rod occurred when the heat rating was increased from 23,7 to 28,3 kW/m (rate for the increase of the heat rate was 1,29 W/m/s). The heat rating was then increased to 30,6 kW/m (rate for the increase of the heat rate 0,23 W/m/s). The very wide opening of the axial crack is due to the swelling of the central part of the high burnup oxide fuel.

1998-11-16

5 Acknowledgement

The neutron radiography at R2 was performed by Ingvar Gustafsson, the gamma measurements and the profilometry were performed by Per Ekberg and the optical microscopy and the SEM examinations were performed by Ove Mattsson. Bengt-Åke Nilsson assisted in the compilation of this report. Their work is gratefully acknowledged.

References

- [1] VANKEERBERGHEN, M
The integral fuel rod behaviour test IFA-597.2: pre-characterisation and analysis of the measurements. HWR-442, March 1996
- [2] VANKEERBERGHEN, M
Fuel rod failure in the integral fuel rod behaviour test IFA-597.2. HWR-466, May 1996
- [3] LYSELL, G and GRIGORIEV, V
Characteristics of axial splits in failed BWR fuel rods, IAEA Technical Committee Meeting on "Fuel Chemistry and Pellet-Clad Interaction Related to High Burnup Fuel" Nyköping, Sweden, 7-11 September 1998

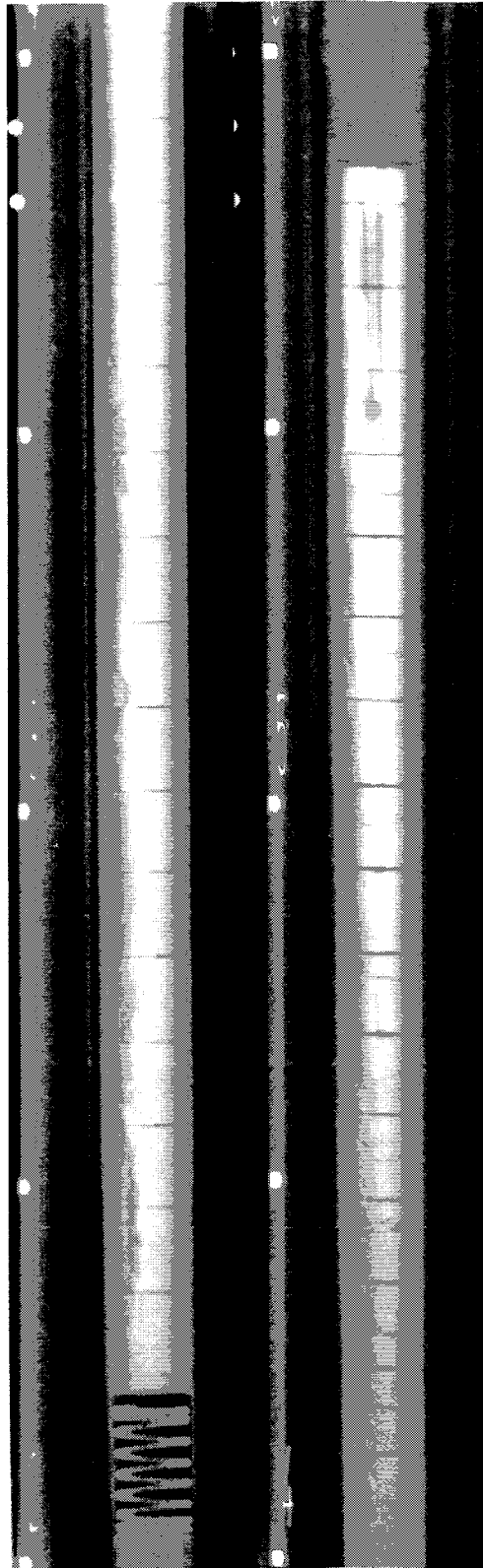
1998-11-16

Table 1

Positions of specimens for destructive examinations.

Axial position (mm from lower end)	Specimen number	Type of examination or comment
135,4		Lower end of cracks
147		Lower end of fuel column
159-175		Part of cladding without oxide and crud
166	1805	Cross section, optical microscopy
~286		Irregularity of axial crack
360-380	1802	Fracture surface, SEM
383	1803	Cross section, SEM
415	1804	Cross section, optical microscopy
473		Lower end of central hole for thermocouple
587-507	1801	Fracture surface, SEM
508		Upper end of fuel column
512,4		Upper end of long axial crack

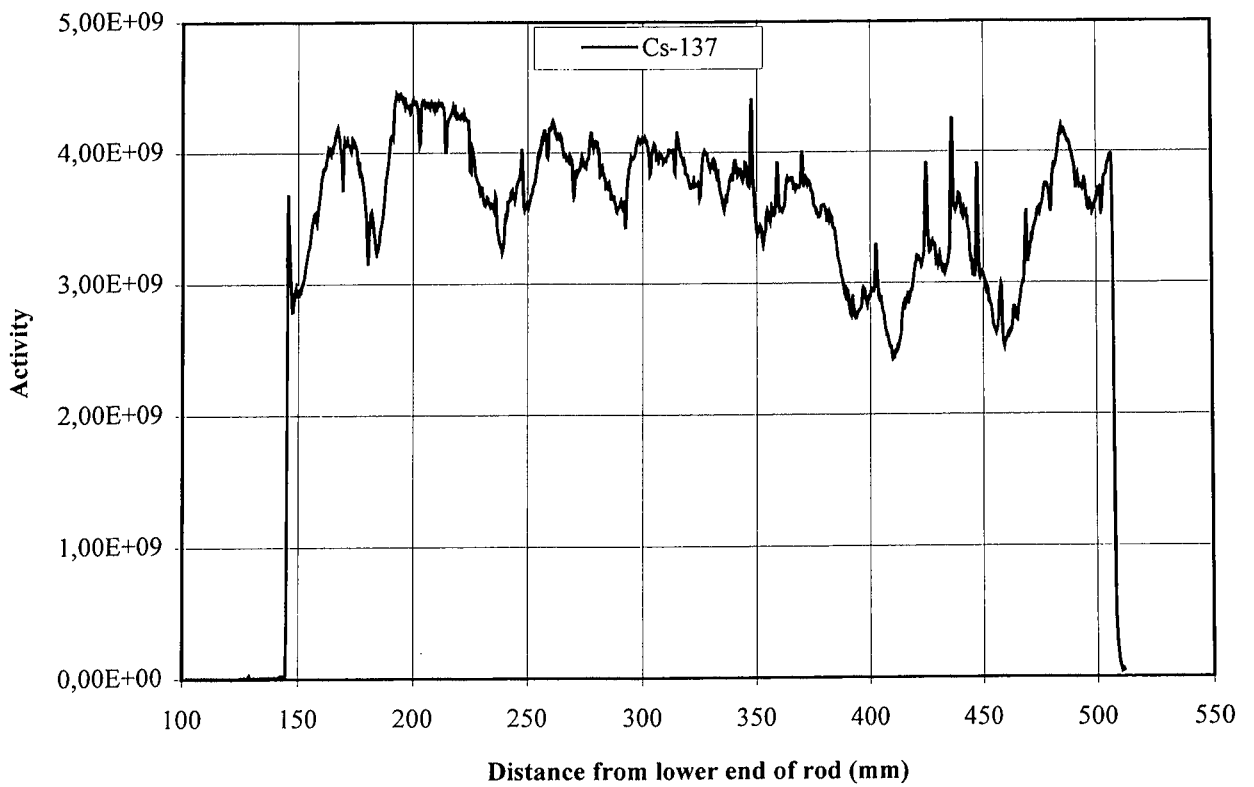
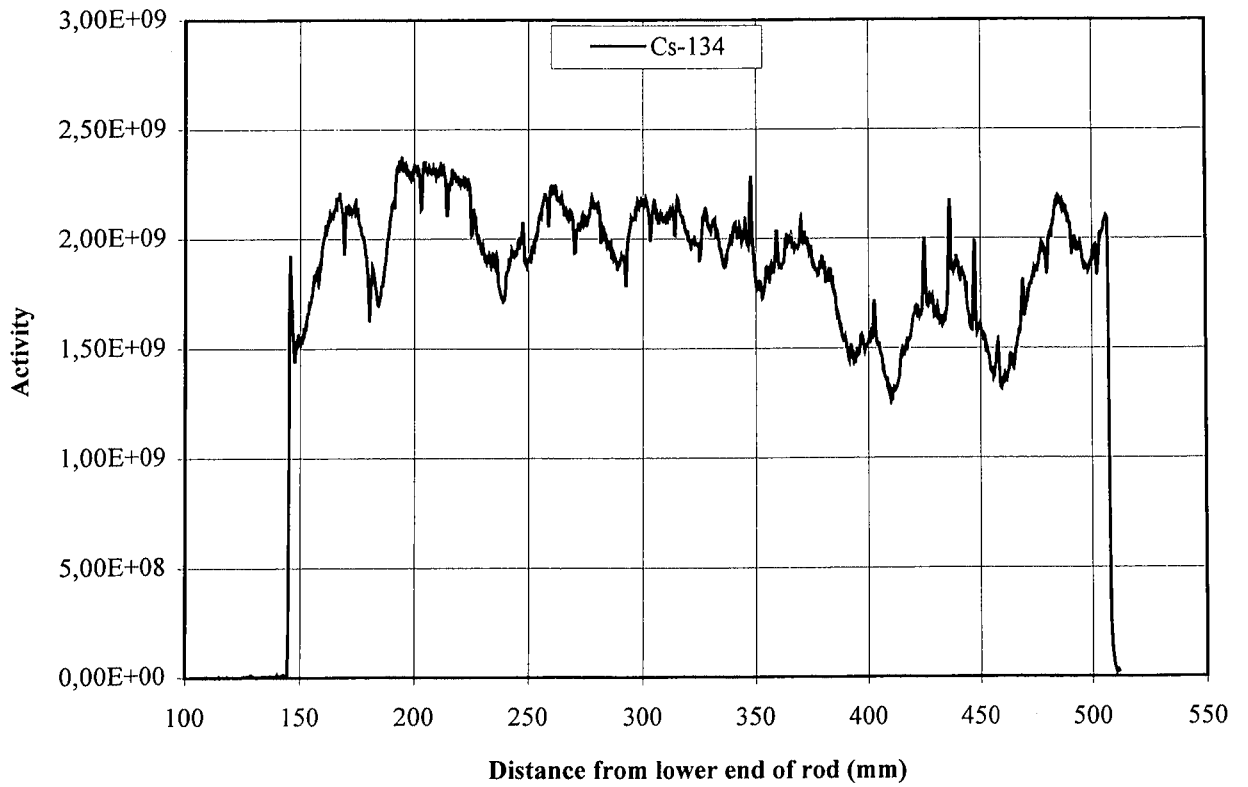
1998-11-16



Appendix A1

Neutron radiography of rod 5 in test IFA-597.2.
The magnification is about 1,01x. Distance between
markings is 50 mm.

1998-11-16



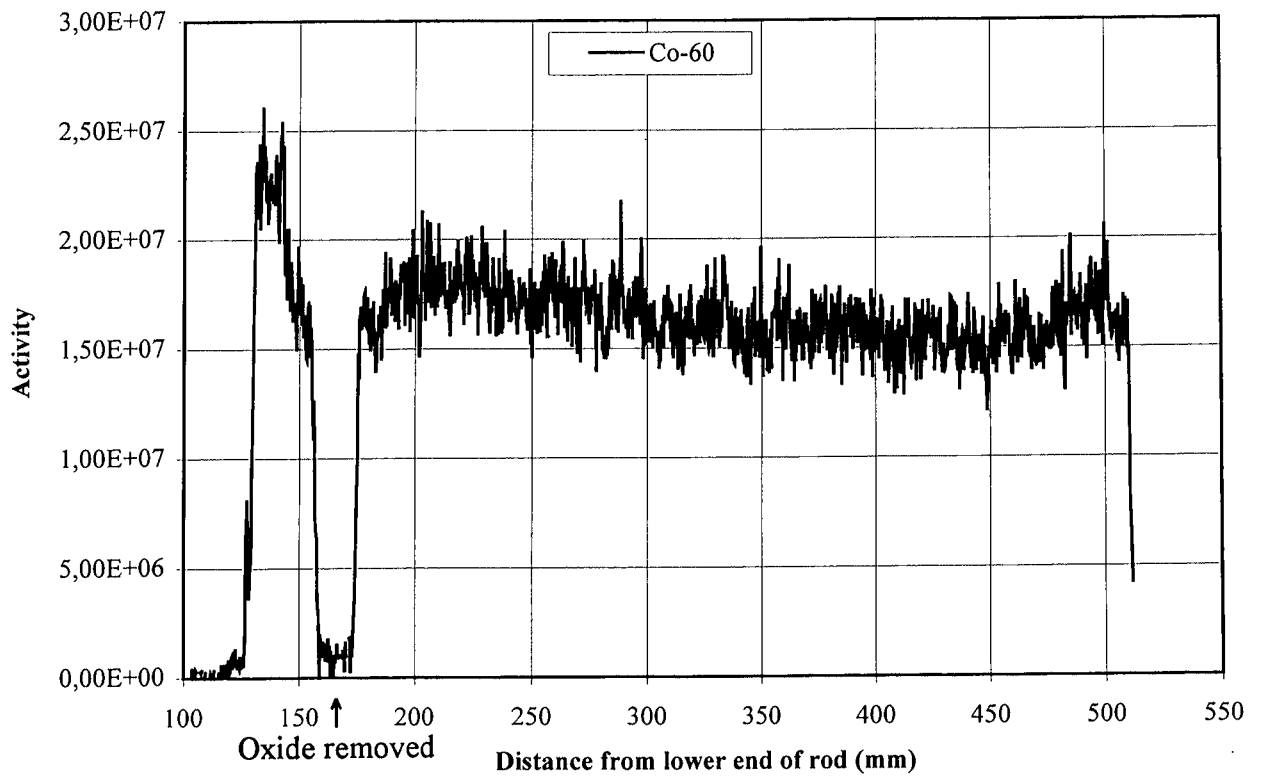
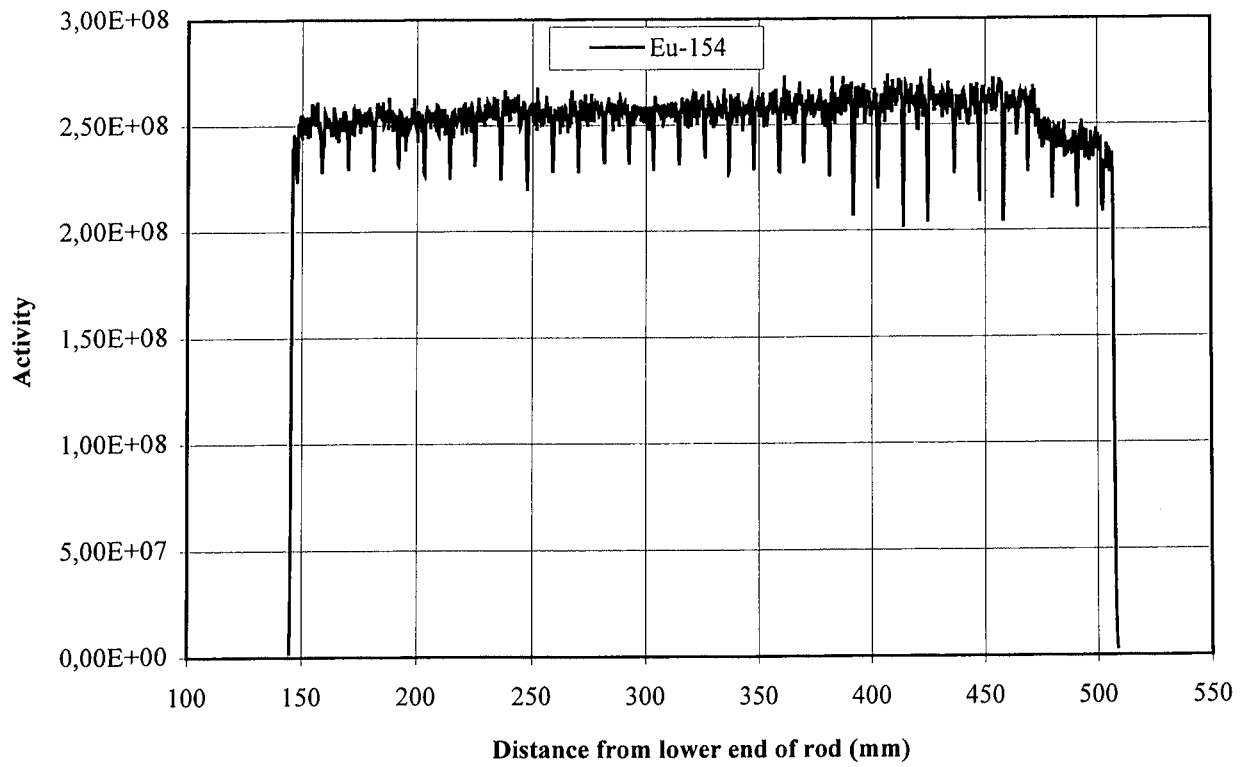
Appendix B1

Axial gamma scanning of rod 5 in test IFA-597.2.

Upper: Cs-134.

Lower: Cs-137.

1998-11-16



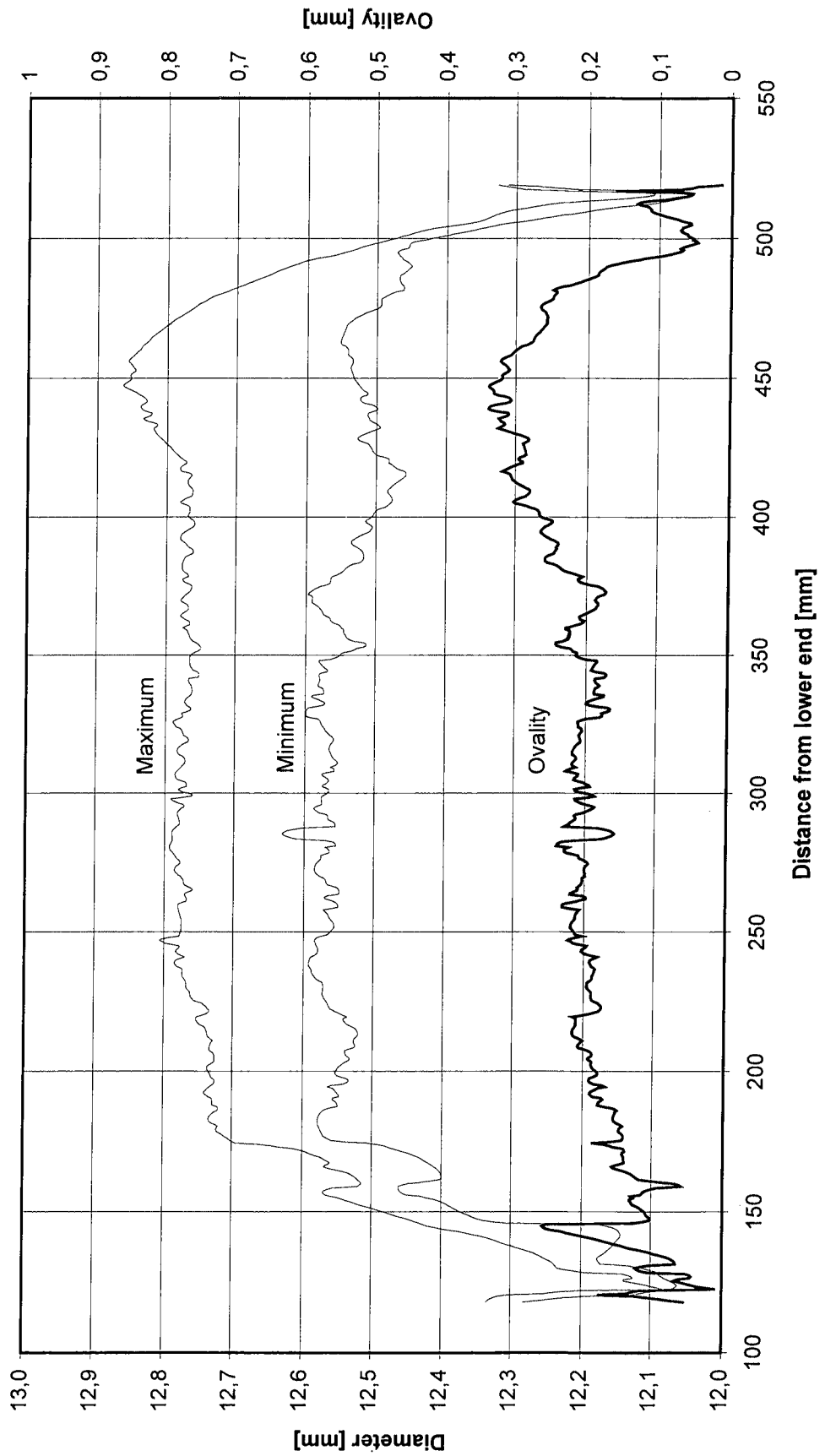
Appendix B2

Axial gamma scanning of rod 5 in test IFA-597.2.

Upper: Eu-154.

Lower: Co-60.

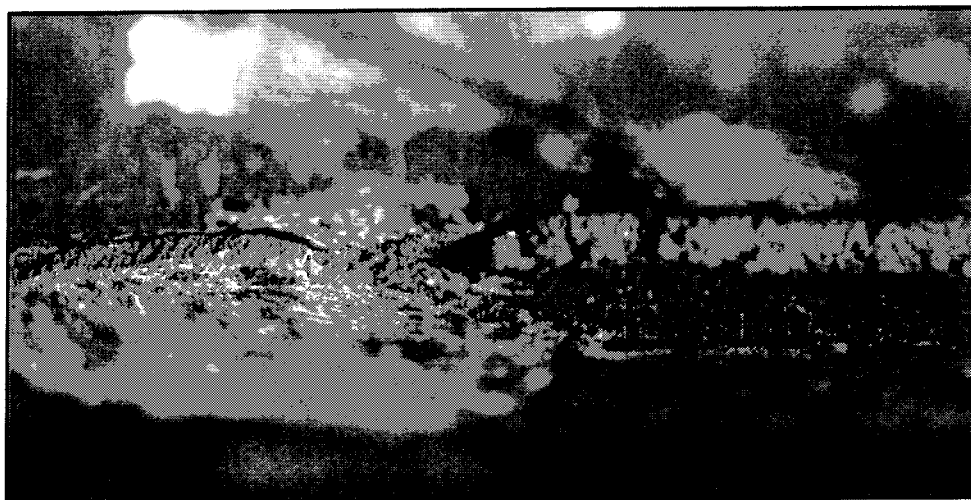
1998-11-16



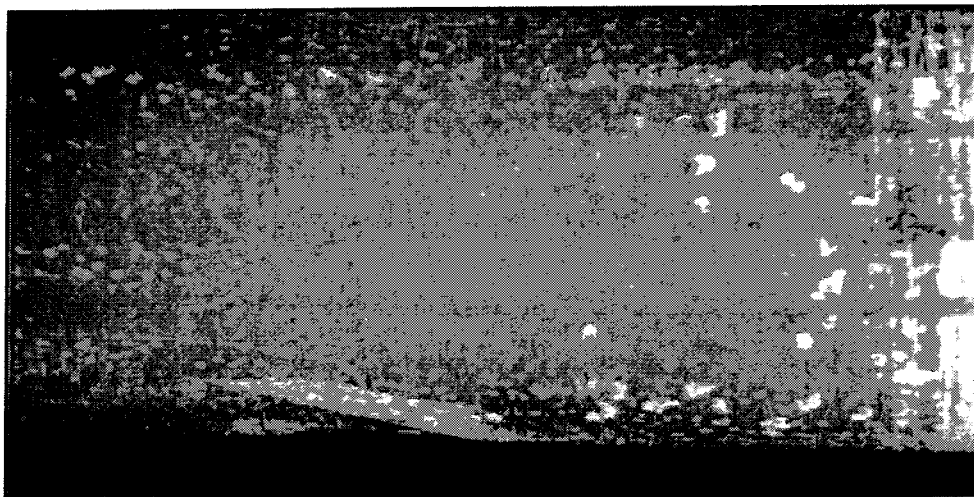
Appendix C2

Profilometry of rod 5 in test IFA-597.2.
Diameter increase (min and max) and ovality.

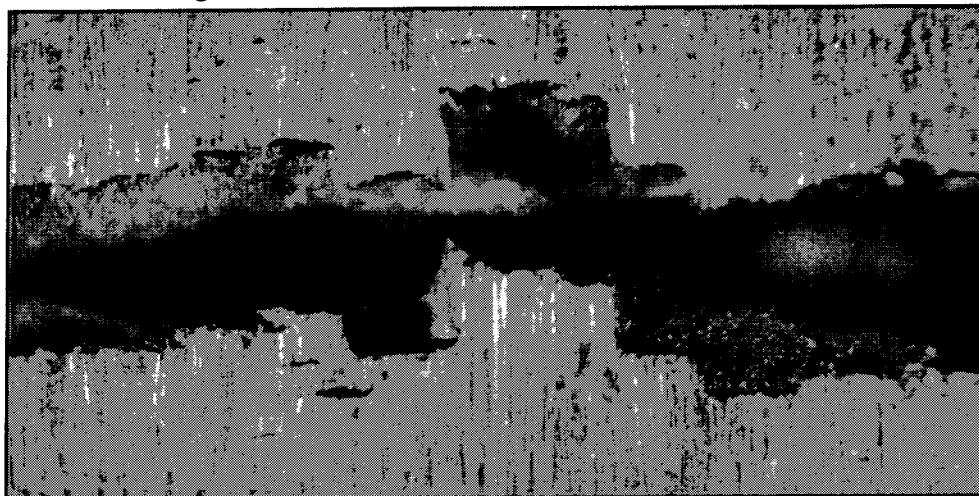
1998-11-16



D5.1 Detail of fracture surface with striations at the position where the crack is branched. 146 mm from rod bottom. Magnification 20x.



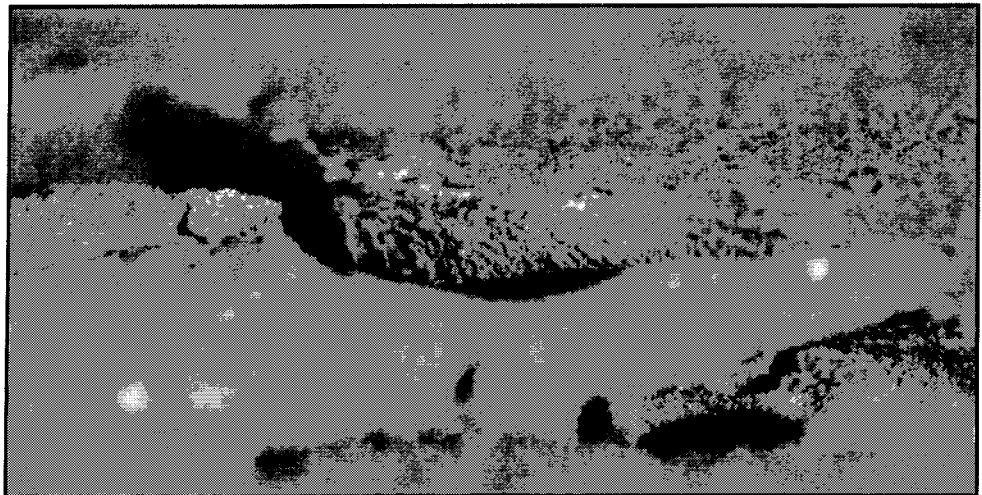
D5.2 Position where the crack is branched. Relative displacement between the sides of the crack indicates some shear component in the cracking mechanism. 146 mm from rod bottom. Magnification 5x.



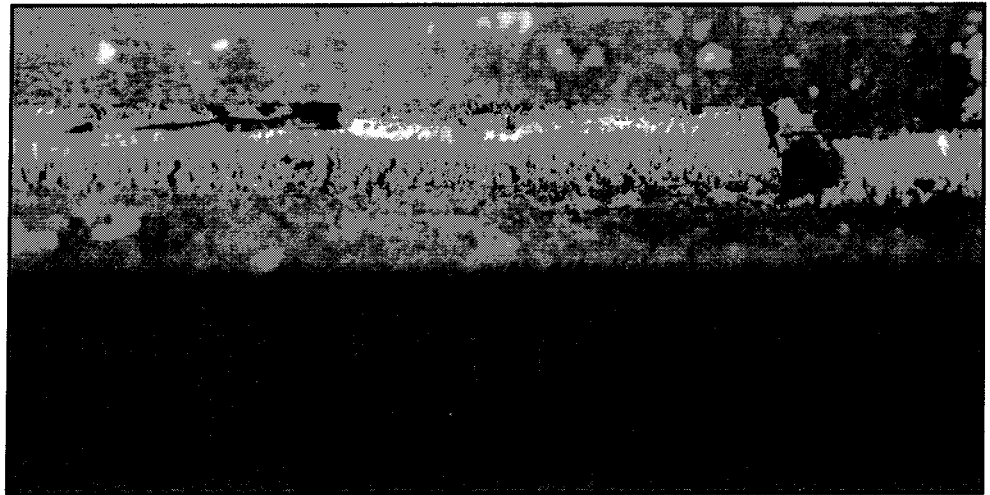
D5.3 Detail at position in the lower part of the rod where the outer oxide layer was removed in connection with refabrication. Observe minor cracks in oxide nodules beside main crack. 166 mm from rod bottom. Magnification 20x.

Appendix D5 Visual inspection of rod 5 in test IFA-597.2.

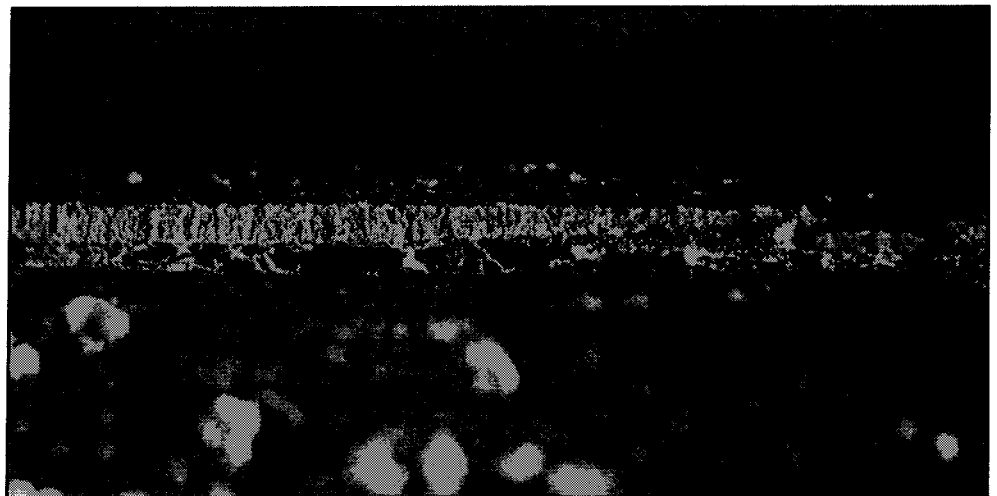
1998-11-16



D6.1 Detail of fracture surface with striations. 286 mm from rod bottom. Magnification 20x.

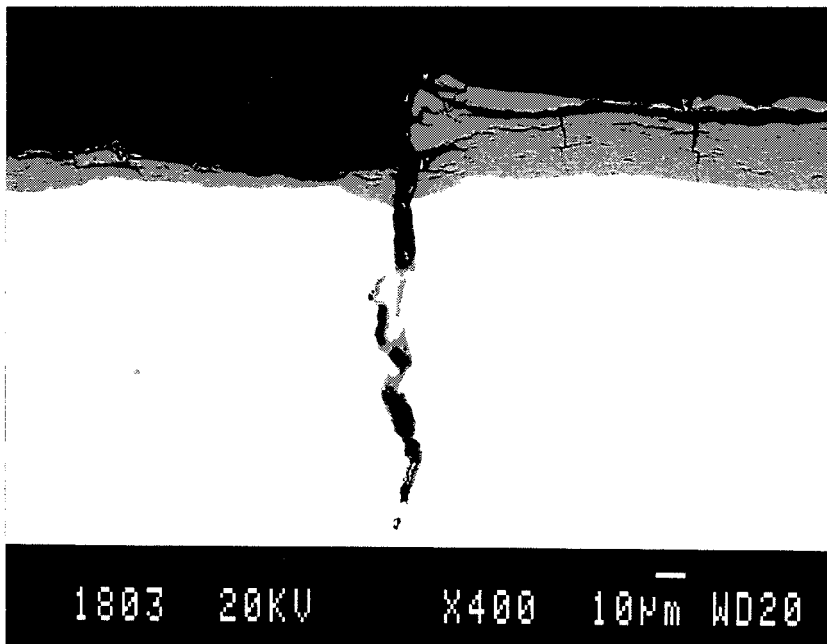


D6.2 Detail of fracture surface. Varying depth of part of fracture surface perpendicular to outer surface of the cladding. 373 mm from rod bottom. Magnification 10x.

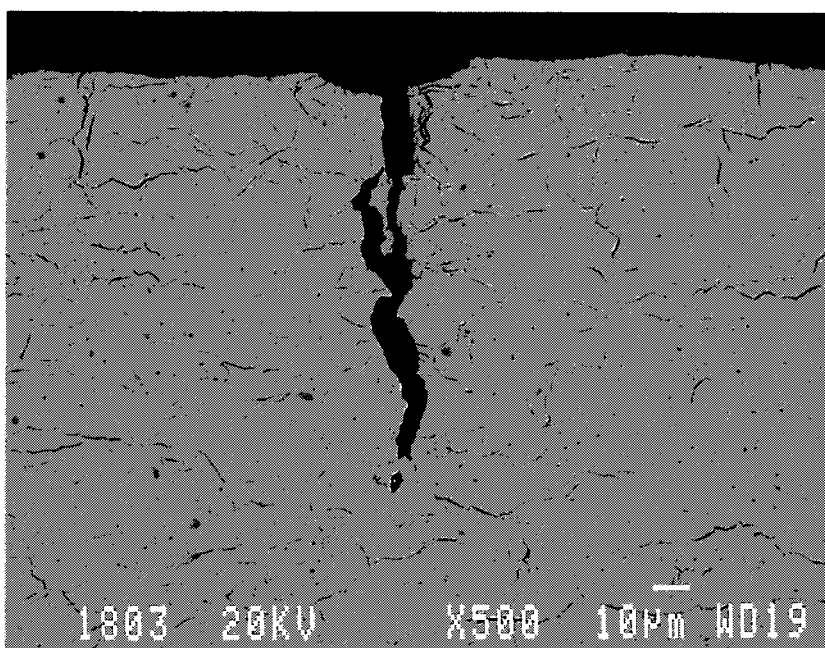


D6.3 Detail of fracture surface. Varying depth of part of fracture surface perpendicular to outer surface of the cladding. 373 mm from rod bottom. Magnification 10x.

1998-11-16



Oxide contrast image. Magnification 400x.

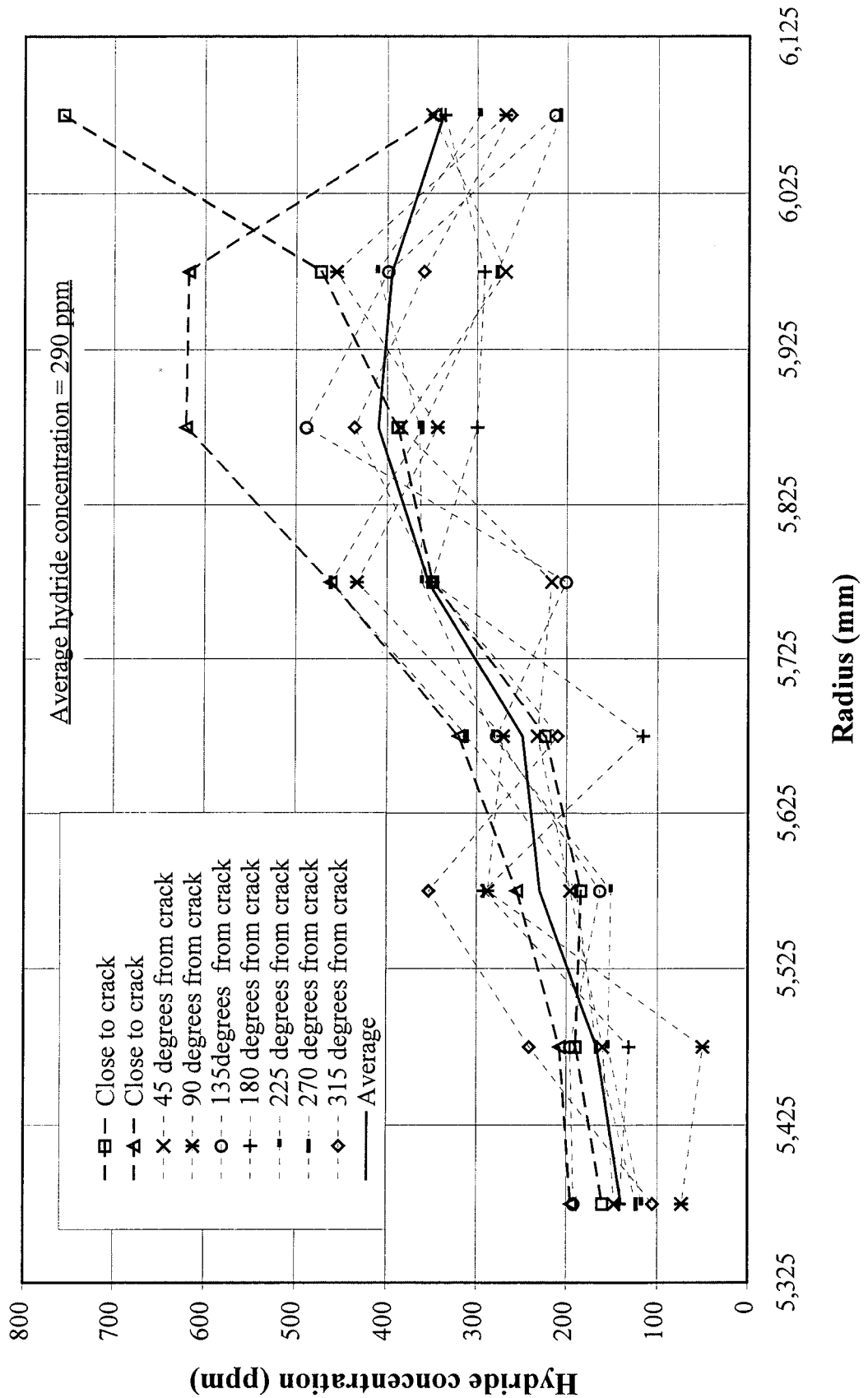


Hydride contrast image. Magnification 500x.

Appendix F5

Scanning electron microscopy of polished cladding surface.
Rod 5 in test IFA-597.2. Specimen 1803, 383 mm from rod bottom.

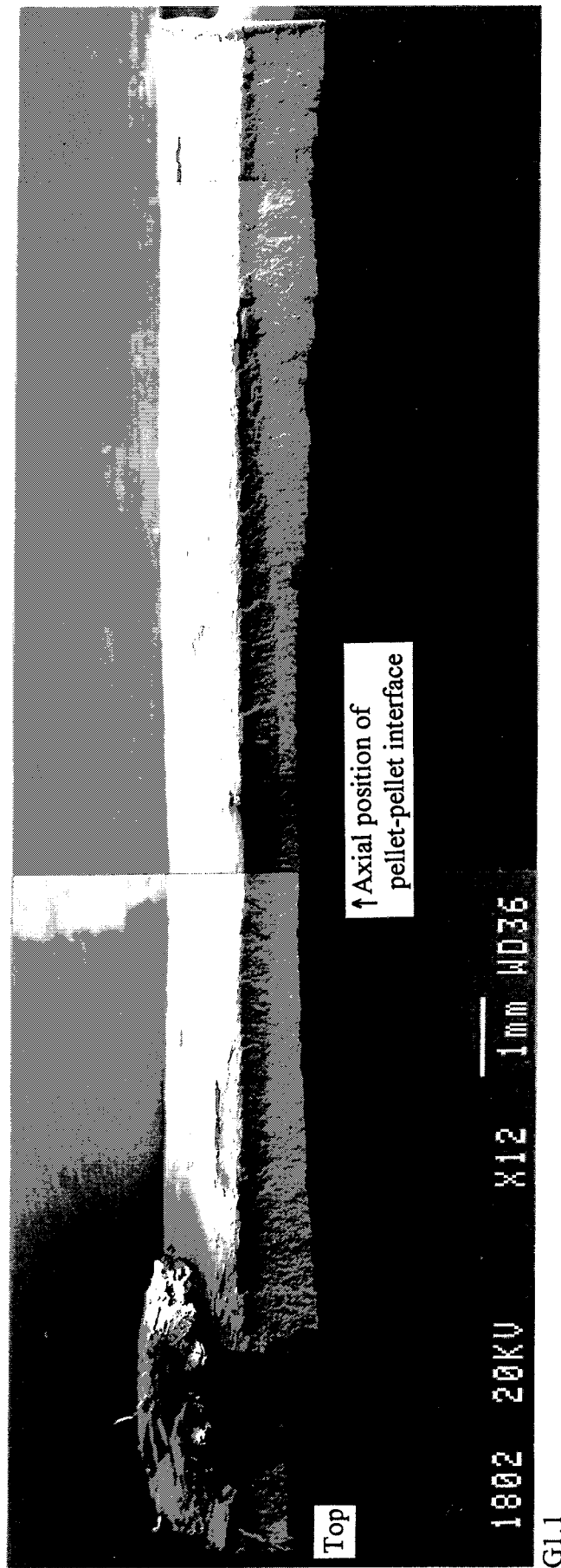
1998-11-16



Appendix F8

Scanning electron microscopy of polished cladding surfaces. Rod 5 in test IFA-597.2. Specimen 1803, 383 mm from rod bottom. Measurements of hydride content at 8 different angular orientations.

1998-11-16

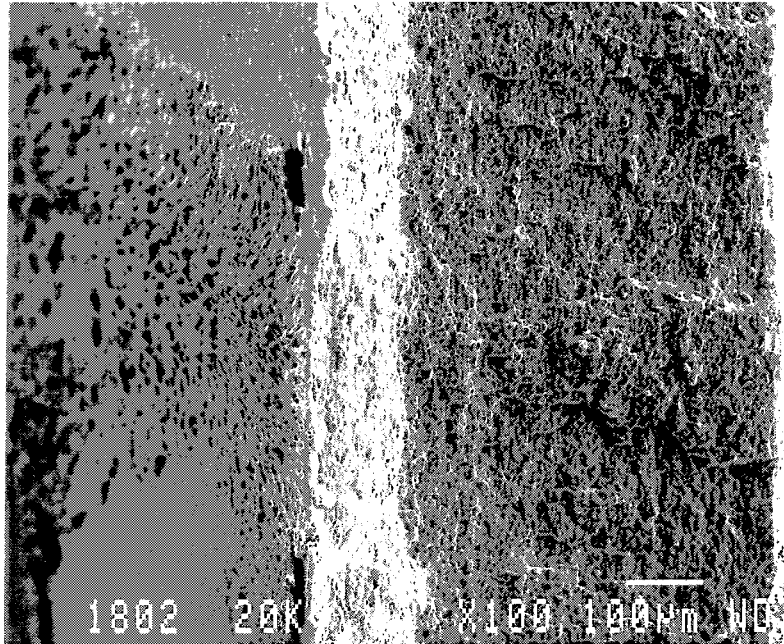


Appendix G1

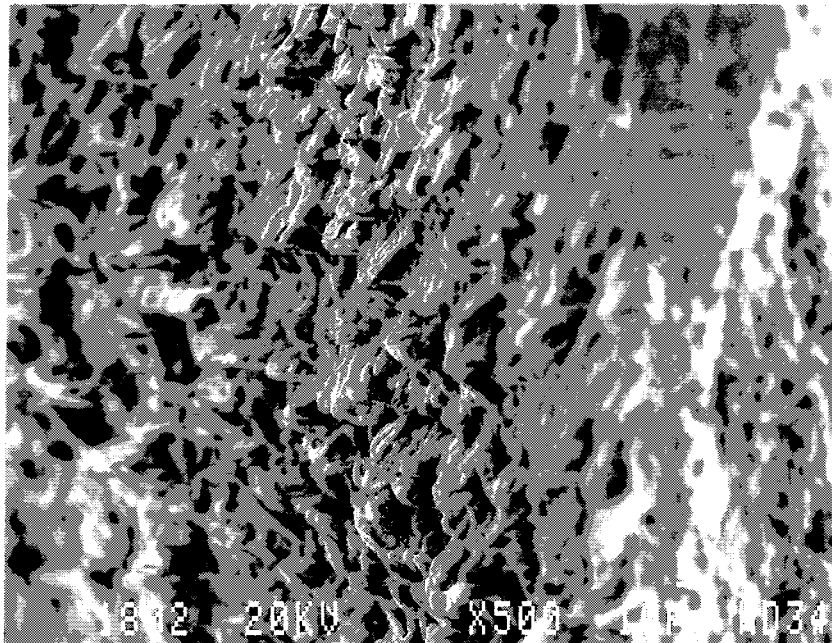
Scanning electron microscopy of cladding fracture surfaces.
Rod 5 in test IFA-597.2. Specimen 1802, 360-380 mm from rod bottom. Overview of specimen.
Magnification 12x.

1998-11-16

Axial direction →



G6.1 Overview of pellet-pellet interface. Magnification 100x.

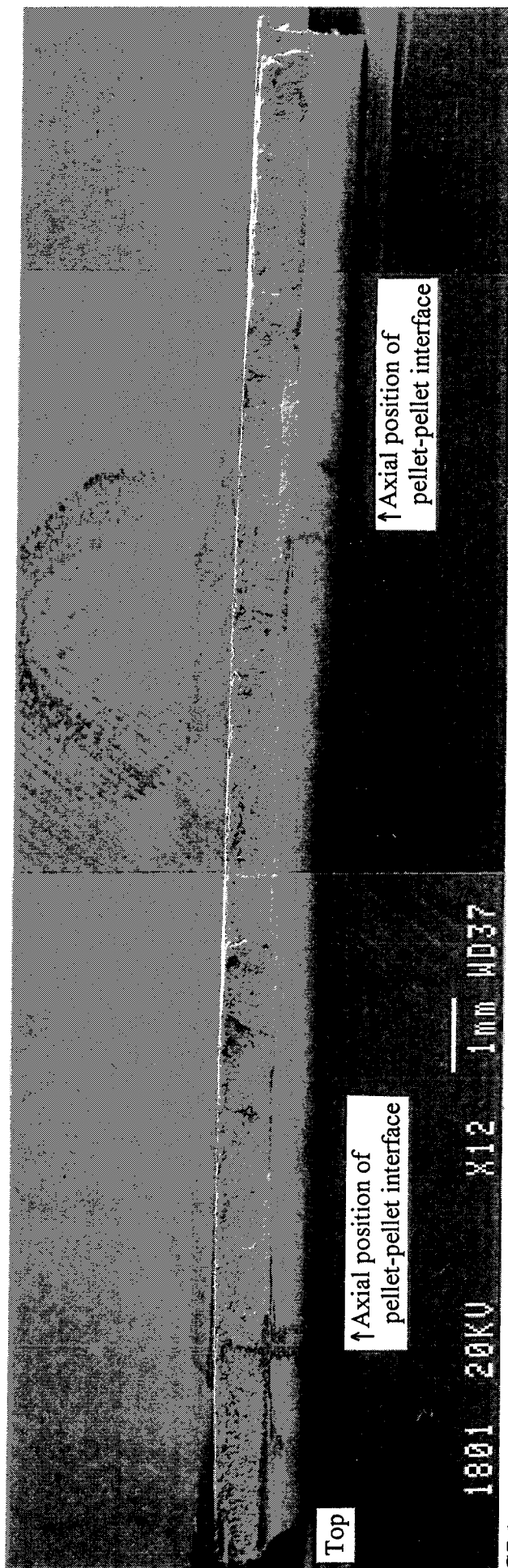


G6.2 Detail of photo G6.1. Magnification 500x.

Appendix G6

Scanning electron microscopy of cladding fracture surfaces. Rod 5 in test IFA-597.2. Specimen 1802. Clad inside oxide at position for pellet-pellet interface. Position see photo G3.1 in Appendix G3.

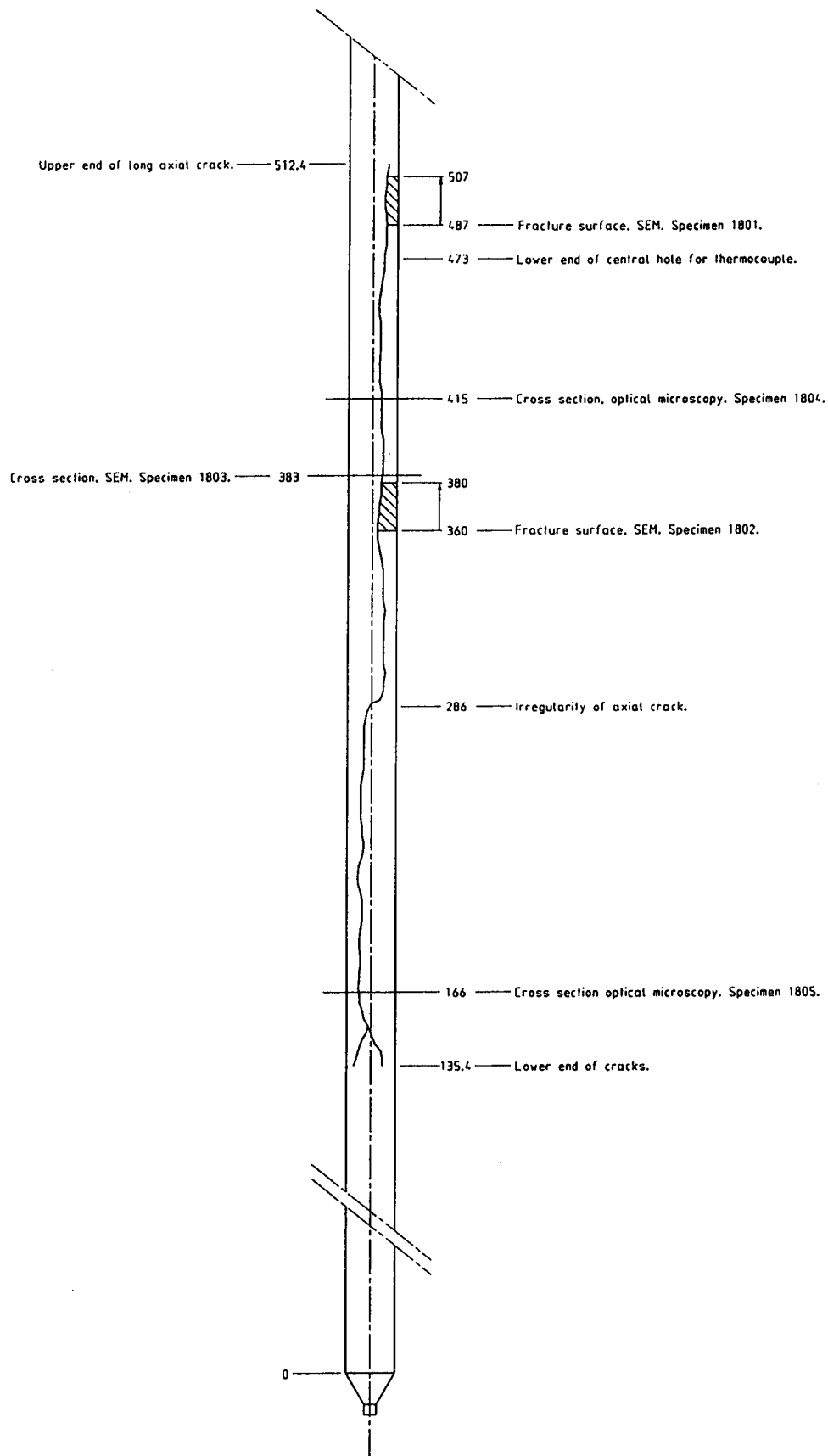
1998-11-16



G7.1

Appendix G7 Scanning electron microscopy of cladding fracture surfaces.
Rod 5 in test IFA-597.2. Specimen 1801, 487-507 mm from rod bottom. Overview of specimen.
Magnification 12x.

1998-11-16



Appendix H1 Positions of specimens for destructive examinations.

www.ski.se

STATENS KÄRNKRAFTINSPEKTION
Swedish Nuclear Power Inspectorate

POST/POSTAL ADDRESS SE-106 58 Stockholm

BESÖK/OFFICE Klarabergsviadukten 90

TELEFON/TELEPHONE +46 (0)8 698 84 00

TELEFAX +46 (0)8 661 90 86

E-POST/E-MAIL ski@ski.se

WEBBPLATS/WEB SITE www.ski.se